Measurements of the Branching Fraction and Polarization in $B^+ \to \rho^+ K^{*0}$ Decays

J. Zhang,[7] K. Abe,[7] I. Adachi,[7] H. Aihara,[42] K. Arinstein,[1] Y. Asano,[46] T. Aushev,[11] T. Aziz,[38] S. Bahinipati,[4] A. M. Bakich,[37] E. Barberio,[19] U. Bitenc,[12] I. Bizjak,[12] S. Blyth,[24] A. Bondar,[1] A. Bozek,[25] J. Brodzicka,[25] T. E. Browder,[6] P. Chang,[24] A. Chen,[22] K.-F. Chen,[24] W. T. Chen,[22] B. G. Cheon,[3] R. Chistov,[11] S.-K. Choi,[5] Y. Choi,[36] Y. K. Choi,[36] A. Chuvikov,[32] S. Cole,[37] J. Dalseno,[19] M. Danilov,[11] M. Dash,[47] J. Dragic,[7] S. Eidelman,[1] F. Fang,[6] S. Fratina,[12] N. Gabyshev,[1] T. Gershon,[7] G. Gokhroo,[38] B. Golob,[17,12] A. Gorišek,[12] T. Hara,[30] M. Hazumi,[7] L. Hinz,[16] T. Hokuue,[20] Y. Hoshi,[40] S. Hou,[22] W.-S. Hou,[24] T. Iijima,[20] A. Imoto,[21] A. Ishikawa,[7] H. Ishino,[43] R. Itoh,[7] M. Iwasaki,[42] J. H. Kang,[48] J. S. Kang,[14] S. U. Kataoka,[21] H. Kawai,[2] T. Kawasaki,[27] H. R. Khan,[43] H. Kichimi,[7] H. J. Kim,[15] S. K. Kim,[35] S. M. Kim,[36] K. Kinoshita,[4] S. Korpar,[18,12] P. Krokovny,[1] C. C. Kuo,[22] Y.-J. Kwon,[48] G. Leder,[10] T. Lesiak,[25] J. Li,[34] A. Limosani,[7] S.-W. Lin,[24] J. MacNaughton,[10] F. Mandl,[10] T. Matsumoto,[44] A. Matyja,[25] Y. Mikami,[41] W. Mitaroff,[10] K. Miyabayashi,[21] H. Miyake,[30] H. Miyata,[27] R. Mizuk,[11] G. R. Moloney,[19] T. Nagamine,[41] Y. Nagasaka,[8] E. Nakano,[29] M. Nakao,[7] H. Nakazawa,[7] Z. Natkaniec,[25] S. Nishida,[7] O. Nitoh,[45] T. Nozaki,[7] S. Ogawa,[39] T. Ohshima,[20] T. Okabe,[20] S. Okuno,[13] S. L. Olsen,[6] Y. Onuki,[27] W. Ostrowicz,[25] H. Ozaki,[7] C. W. Park,[36] L. S. Peak,[37] R. Pestotnik,[12] L. E. Piilonen,[47] H. Sagawa,[7] Y. Sakai,[7] T. R. Sarangi,[7] T. Schietinger,[16] O. Schneider,[16] A. J. Schwartz,[4] M. E. Sevior,[19] H. Shibuya,[39] A. Somov,[4] R. Stamen,[7] S. Stanič,[28] M. Starič,[12] T. Sumiyoshi,[44] S. Suzuki,[33] O. Tajima,[7] F. Takasaki,[7] M. Tanaka,[7] Y. Teramoto,[29] X. C. Tian,[31] T. Tsuboyama,[7] T. Tsukamoto,[7] S. Uehara,[7] T. Uglov,[11] K. Ueno,[24] S. Uno,[7] P. Urquijo,[19] G. Varner,[6] K. E. Varvell,[37] S. Villa,[16] C. C. Wang,[24] C. H. Wang,[23] M.-Z. Wang,[24] Y. Watanabe,[43] Q. L. Xie,[9] B. D. Yabsley,[47] A. Yamaguchi,[41] Y. Yamashita,[26] Heyoung Yang,[35] J. Ying,[31] L. M. Zhang,[34] Z. P. Zhang,[34] and D. Žontar[17,12]

(Belle Collaboration)

[1]*Budker Institute of Nuclear Physics, Novosibirsk*
[2]*Chiba University, Chiba*
[3]*Chonnam National University, Kwangju*
[4]*University of Cincinnati, Cincinnati, Ohio 45221*
[5]*Gyeongsang National University, Chinju*
[6]*University of Hawaii, Honolulu, Hawaii 96822*
[7]*High Energy Accelerator Research Organization (KEK), Tsukuba*
[8]*Hiroshima Institute of Technology, Hiroshima*
[9]*Institute of High Energy Physics, Chinese Academy of Sciences, Beijing*
[10]*Institute of High Energy Physics, Vienna*
[11]*Institute for Theoretical and Experimental Physics, Moscow*
[12]*J. Stefan Institute, Ljubljana*
[13]*Kanagawa University, Yokohama*
[14]*Korea University, Seoul*
[15]*Kyungpook National University, Taegu*
[16]*Swiss Federal Institute of Technology of Lausanne, EPFL, Lausanne*
[17]*University of Ljubljana, Ljubljana*
[18]*University of Maribor, Maribor*
[19]*University of Melbourne, Victoria*
[20]*Nagoya University, Nagoya*
[21]*Nara Women's University, Nara*
[22]*National Central University, Chung-li*
[23]*National United University, Miao Li*
[24]*Department of Physics, National Taiwan University, Taipei*
[25]*H. Niewodniczanski Institute of Nuclear Physics, Krakow*
[26]*Nippon Dental University, Niigata*
[27]*Niigata University, Niigata*
[28]*Nova Gorica Polytechnic, Nova Gorica*
[29]*Osaka City University, Osaka*
[30]*Osaka University, Osaka*
[31]*Peking University, Beijing*
[32]*Princeton University, Princeton, New Jersey 08544*
[33]*Saga University, Saga*

[34]University of Science and Technology of China, Hefei
[35]Seoul National University, Seoul
[36]Sungkyunkwan University, Suwon
[37]University of Sydney, Sydney NSW
[38]Tata Institute of Fundamental Research, Bombay
[39]Toho University, Funabashi
[40]Tohoku Gakuin University, Tagajo
[41]Tohoku University, Sendai
[42]Department of Physics, University of Tokyo, Tokyo
[43]Tokyo Institute of Technology, Tokyo
[44]Tokyo Metropolitan University, Tokyo
[45]Tokyo University of Agriculture and Technology, Tokyo
[46]University of Tsukuba, Tsukuba
[47]Virginia Polytechnic Institute and State University, Blacksburg, Virginia 24061
[48]Yonsei University, Seoul

(Received 14 May 2005; published 28 September 2005)

We present the results of a study of the charmless vector-vector decay $B^+ \to \rho^+ K^{*0}$, based on 253 fb^{-1} of data collected with the Belle detector at the KEKB asymmetric-energy e^+e^- collider. We obtain the branching fraction $\mathcal{B}(B^+ \to \rho^+ K^{*0}) = [8.9 \pm 1.7(\text{stat}) \pm 1.2(\text{syst})] \times 10^{-6}$. We also perform a helicity analysis of the ρ and K^* vector mesons, and obtain the longitudinal polarization fraction $f_L(B^+ \to \rho^+ K^{*0}) = 0.43 \pm 0.11(\text{stat})^{+0.05}_{-0.02}(\text{syst})$.

DOI: 10.1103/PhysRevLett.95.141801 PACS numbers: 13.25.Hw, 12.39.St, 13.88.+e, 14.40.Nd

The standard model (SM) predicts that the longitudinal polarization fraction (f_L) in B meson decays to light vector-vector (VV) final states is close to unity [1]. In the tree dominated $B^+ \to \rho^+\rho^0$ and $B^0 \to \rho^+\rho^-$ decays, this prediction has been confirmed [2–4]. In contrast, for the pure $b \to s$ penguin $B \to \phi K^*$ decay, Belle [5] and *BABAR* [4] have found that the longitudinal and transverse polarization fractions are comparable, which is in disagreement with the expectation. Possible explanations for this discrepancy include enhanced nonfactorizable contributions such as penguin annihilation [1], large $SU(3)$ breaking in form factors [6], or new physics [7,8]. It is therefore important to perform polarization measurements in other VV modes, in particular, in the pure penguin $b \to s\bar{d}d$ decay $B^+ \to \rho^+ K^{*0}$.

In this Letter, we present the results of a study of $B^+ \to \rho^+ K^{*0}$ decays [9] with a 253 fb^{-1} data sample containing 275×10^6 B meson pairs collected with the Belle detector at the KEKB asymmetric-energy e^+e^- collider [10] operating at the $\Upsilon(4S)$ resonance ($\sqrt{s} = 10.58$ GeV). The production rates for B^+B^- and $B^0\bar{B}^0$ pairs are assumed to be equal.

The Belle detector is a large solid-angle magnetic spectrometer that consists of a silicon vertex detector (SVD), a 50-layer central drift chamber (CDC), an array of aerogel threshold Čerenkov counters (ACC), a barrel-like arrangement of time-of-flight scintillation counters (TOF), and an electromagnetic calorimeter comprised of CsI(Tl) crystals (ECL) located inside a superconducting solenoid coil that provides a 1.5 T magnetic field. An iron flux return located outside of the coil is instrumented to detect K^0_L mesons and to identify muons (KLM). The detector is described in detail elsewhere [11].

We dectect ρ^+ mesons decaying to $\pi^+\pi^0$ and K^{*0} mesons decaying to $K^+\pi^-$. We select $B^+ \to \rho^+ K^{*0}$ candidate events by combining three charged tracks (two oppositely charged pions and one kaon) and one neutral pion. Each charged track is required to have a transverse momentum $p_T > 0.1$ GeV/c and to have an origin within 0.2 cm in the radial direction and 5 cm along the beam direction of the interaction point (IP).

Particle identification likelihoods for the pion and kaon hypotheses are calculated by combining information from the TOF and ACC systems with dE/dx measurements in the CDC. Similarly, electrons are identified by means of a likelihood based on ECL measurements, dE/dx information from the CDC, and the responses of the ACC. To identify kaons, we require the kaon likelihood ratio, $L_K/(L_K + L_\pi)$, to be greater than 0.6. To identify pions, we require $L_K/(L_K + L_\pi)$ to be less than 0.4. The efficiency for this selection is 86% for kaons and 89% for pions, with corresponding π/K misidentification rates of 8% and 10%. In addition, charged tracks are rejected if they are consistent with an electron hypothesis.

Candidate π^0 mesons are reconstructed from pairs of photons that have an invariant mass in the range 0.1178–0.1502 GeV/c^2, corresponding to a window of $\pm 3\sigma$ around the nominal π^0 mass. The photons are assumed to originate from the IP. The energy of each photon in the laboratory frame is required to be greater than 50 MeV for the ECL barrel region ($32° < \theta < 129°$) and 100 MeV for the ECL end cap regions ($17° < \theta < 32°$ and $129° < \theta < 150°$), where θ denotes the polar angle of the photon with respect to the beam line. The π^0 candidates are kinematically constrained to the nominal π^0 mass. In order to reduce the combinatorial background, we only

accept π^0 candidates with momenta $p_{\pi^0} > 0.40$ GeV/c in the e^+e^- center-of-mass (c.m.) system.

Candidate ρ^+ mesons are $\pi^+\pi^0$ pairs with an invariant mass in the region $0.62\ \mathrm{GeV}/c^2 < M(\pi^+\pi^0) < 0.92\ \mathrm{GeV}/c^2$. Candidate K^{*0} mesons are $K^+\pi^-$ pairs with an invariant mass $0.83\ \mathrm{GeV}/c^2 < M(K^+\pi^-) < 0.97\ \mathrm{GeV}/c^2$.

To isolate the signal, we form the beam-constrained mass $M_{\mathrm{bc}} \equiv \sqrt{E^2_{\mathrm{beam}} - p^2_B}$, and the energy difference $\Delta E \equiv E_B - E_{\mathrm{beam}}$, where E_{beam} is the c.m. beam energy, and p_B and E_B are the c.m. momentum and energy, respectively, of the B candidate. The ΔE distribution has a tail on the lower side caused by incomplete longitudinal containment of electromagnetic showers in the CsI(Tl) crystals. We accept events in the region $M_{\mathrm{bc}} > 5.2\ \mathrm{GeV}/c^2$ and $-0.3\ \mathrm{GeV} < \Delta E < 0.3\ \mathrm{GeV}$, and define a signal region in M_{bc} and ΔE as $5.27\ \mathrm{GeV}/c^2 < M_{\mathrm{bc}} < 5.29\ \mathrm{GeV}/c^2$ and $-0.10\ \mathrm{GeV} < \Delta E < 0.06\ \mathrm{GeV}$ respectively. These requirements correspond to approximately $\pm 3\sigma$ for both quantities.

The continuum process $e^+e^- \to q\bar{q}$ ($q = u, d, s, c$) is the main source of background and must be strongly suppressed. One method of discriminating the signal from continuum is based on the event topology, which tends to be isotropic for $B\bar{B}$ events and jetlike for $q\bar{q}$ events. Another discriminating characteristic is θ_B, the c.m. polar angle of the B flight direction. B mesons are produced with a $1 - \cos^2\theta_B$ distribution while continuum background events tend to be uniform in $\cos\theta_B$. The displacement along the beam direction between the signal B vertex and that of the other B, Δz, also provides separation. For B events, the average value of Δz is approximately 200 μm, while continuum events have a common vertex. Additional discrimination is provided by the b-flavor tagging algorithm [12] developed for time-dependent analysis at Belle. The flavor tagging procedure yields two outputs: q ($= \pm 1$), which indicate the flavor of the tagging B, and r, which ranges from 0 to 1 and is a measure of the likelihood that the b flavor of the accompanying B meson is correctly assigned. For signal events, q is more likely consistent with the opposite of the charge of signal B; there is no correlation for continuum events. Events with high values of r are well tagged and are less likely to originate from continuum production. Thus, the quantity qrC_B, where C_B is the charge of the signal B, can be used to discriminate against continuum events.

We use Monte Carlo (MC) simulated signal and data sideband (defined as $5.2\ \mathrm{GeV}/c^2 < M_{\mathrm{bc}} < 5.26\ \mathrm{GeV}/c^2$) events to form a Fisher discriminant based on a set of modified Fox-Wolfram moments [13] that are confirmed to be uncorrelated with M_{bc}, ΔE, and variables considered later in the analysis. Probability density functions (PDFs) derived from the Fisher discriminant, the $\cos\theta_B$ distributions, and the Δz distributions are multiplied to form likelihood functions for signal ($\mathcal{L}_s$) and continuum background ($\mathcal{L}_{q\bar{q}}$); these are combined into a likelihood ratio $\mathcal{R}_s = \mathcal{L}_s/(\mathcal{L}_s + \mathcal{L}_{q\bar{q}})$. We achieve background suppression by imposing qrC_B-dependent $\mathcal{R}_s$ requirements, which are determined by optimizing the figure of merit, $S/\sqrt{S+B}$, where S (B) is the number of signal (background) events in the signal region. A branching fraction of $\mathcal{B}(B^+ \to \rho^+ K^{*0}) = 1 \times 10^{-5}$ is assumed. This requirement removes 99.3% of the continuum background while retaining 41% of the $B^+ \to \rho^+ K^{*0}$ events. The MC-determined efficiency with all selection criteria imposed is 2.7% for longitudinal polarization (A_0) and 4.0% for transverse polarization ($A_\pm$).

The fraction of multiple candidates in the signal region for signal MC events is 3.6% for the A_0 helicity state and 1.7% for the $A_\pm$ state. We allow multiple candidates in this analysis.

To investigate backgrounds from $b \to c$ decays, we use a sample of $B\bar{B}$ MC events corresponding to an integrated luminosity of 412 fb^{-1}. We find a contribution from $B^+ \to \bar{D}^0(K^+\pi^-\pi^0)\pi^+$ decays in the ρ or K^* sideband region and require $|M(K\pi\pi^0) - M_{D^0}| > 0.050\ \mathrm{GeV}/c^2$ to veto these events. This requirement does not remove any $B^+ \to \rho^+ K^{*0}$ events. Among the charmless B decays, potential backgrounds arise from $B^+ \to a_1^0 K^+$, $B^+ \to \rho^+ K_0^*(1430)$, nonresonant $B^+ \to \rho^+ K^+ \pi^-$, and $B^+ \to K^{*0}\pi^+\pi^0$. We separate the signal from these backgrounds by fitting the ρ and K^* invariant mass distributions.

We extract the signal yield by applying an extended unbinned maximum-likelihood fit to the two-dimensional M_{bc}-ΔE distribution. The fit includes components for the signal (of which 14.8% involve incorrect combinations) and backgrounds from both continuum events and $b \to c$ decays. The PDFs for signal and $b \to c$ decay are modeled by smoothed two-dimensional histograms obtained from large MC samples. The signal PDF is adjusted to account for small differences observed between data and MC calculations for a high-statistics mode containing π^0 mesons, $B^+ \to \bar{D}^0(K^+\pi^-\pi^0)\pi^+$. The continuum PDF is described by a product of a threshold (ARGUS) function [14] for M_{bc} and a first-order polynomial for ΔE, with shape parameters allowed to vary. All normalizations are allowed to float. Figure 1 shows the final event sample and the fit results. The five-parameter (three normalizations plus two shape parameters for continuum) fit yields 134.8 ± 16.9 $B^+ \to K^+\pi^-\pi^+\pi^0$ events.

We further distinguish the $\rho^+ K^{*0}$ signal from nonresonant decays such as $B^+ \to \rho^+ K^+ \pi^-$ or $B^+ \to K^{*0}\pi^+\pi^0$ by relaxing the $M(\pi^+\pi^0)$ or $M(K^+\pi^-)$ requirements and fitting the $M(\pi^+\pi^0)$ and $M(K^+\pi^-)$ invariant mass distributions. The signal yields obtained from the M_{bc}-ΔE fit for different $M(\pi\pi)$ and $M(K\pi)$ bins are plotted in Fig. 2, where the $M(\pi\pi)$ distribution is for events in the K^* region [$0.83\ \mathrm{GeV}/c^2 < M(K\pi) < 0.97\ \mathrm{GeV}/c^2$] and the $M(K\pi)$ distribution is for events in the ρ region [$0.62\ \mathrm{GeV}/c^2 < M(\pi\pi) < 0.92\ \mathrm{GeV}/c^2$]. We perform separate χ^2 fits to the $M(\pi\pi)$ or $M(K\pi)$ distributions. Each fit includes components for signal and nonresonant background. The

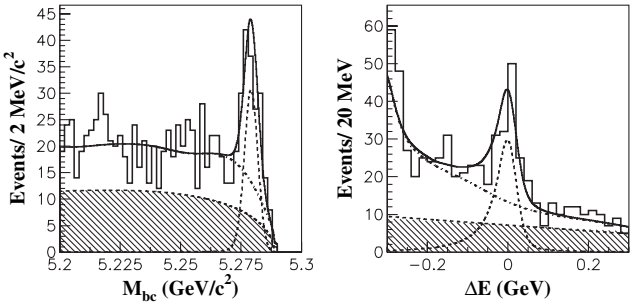

FIG. 1. Projections of $M_{\rm bc}$ for events in the ΔE signal region (left), and projection of ΔE in the $M_{\rm bc}$ signal region (right). The solid curves show the results of the fit. The hatched histograms represent the continuum background. The sum of the $b \to c$ and continuum background component is shown as dot-dashed lines.

signal ρ and K^* PDFs are modeled by relativistic P-wave Breit-Wigner functions with means and widths fixed at their known values [15]; the PDFs are convolved with a Gaussian of $\sigma = 5.3$ MeV, which is obtained by fitting the $D^0(K^-\pi^+)$ invariant mass, to account for the detector resolution. The nonresonant component is represented by a threshold function with parameters determined from MC events where the final states are distributed uniformly over phase space. The $M(\pi\pi)$ mass fit gives 125.4 ± 15.8 ρ and -0.3 ± 3.0 nonresonant $K^{*0}\pi^+\pi^0$ events in the ρ mass region. In the $M(K\pi)$ fit, we find 85.4 ± 16.1 ρK^* signal and 28.8 ± 4.1 nonresonant events in the K^* mass region. The statistical significance of the $B^+ \to \rho^+ K^{*0}$ signal, defined as $\sqrt{\chi^2_0 - \chi^2_{\rm min}}$, where $\chi^2_{\rm min}$ is the χ^2 value at the best-fit signal yield and χ^2_0 is the value with the K^{*0} signal yield set to zero, is 5.3σ (5.2σ with the inclusion of systematics). The contribution from nonresonant $\rho^+ K^+\pi^-$ is significant and is taken into account in both the branching fraction and polarization determinations, while we neglect the nonresonant $K^{*0}\pi^+\pi^0$ contribution.

The fit procedure is checked by using an ensemble of GEANT-simulated pseudo-experiments. By applying the same fit procedure to these samples, we obtain a signal yield of 110.6 ± 7.8 events, while the expectation is 110 events. The 7.1% uncertainty in this check is included in the systematic error.

We use the $\rho^+ \to \pi^+\pi^0$ and $K^{*0} \to K^+\pi^-$ helicity-angle $(\theta_\rho, \theta_{K^*})$ distributions to determine the relative strengths of $|A_0|^2$ and $|A_\pm|^2$. Here θ_ρ (θ_{K^*}) is the angle between an axis antiparallel to the B flight direction and the π^+ (K^+) flight direction in the $\rho(K^*)$ rest frame. For the longitudinal polarization case, the distribution is proportional to $\cos^2\theta_\rho \cos^2\theta_{K^*}$, and for the transverse polarization case, it is proportional to $\sin^2\theta_\rho \sin^2\theta_{K^*}$ [16]. Figure 3 shows the signal yields obtained from $M_{\rm bc}$-ΔE fits in bins of the cosine of the helicity angle for ρ and K^*. We perform a binned simultaneous χ^2 fit to the ρ and K^* helicity-angle distributions. The fit includes components for signal and nonresonant $\rho K\pi$. PDFs for signal A_0 and $A_\pm$ helicity states are determined from the MC simulation. The helicity-angle distribution for data in the high $M(K\pi)$ sideband region $1.1\ {\rm GeV}/c^2 < M(K\pi) < 1.5\ {\rm GeV}/c^2$, where $\rho K\pi$ events dominate, can be fitted by a $\cos^2\theta_\rho$ and a flat $\cos\theta_{K^*}$ distribution with a χ^2/dgf of 10.6/9 (A fit to the ρ helicity distribution with a $\cos^2\theta$ and a flat component gives a flat component fraction of 0.2 ± 0.1). Thus, we assume an S-wave $K\pi$ system and model the nonresonant $B \to \rho K\pi$ PDF based on the MC simulation. The fraction of the nonresonant component is fixed at the values obtained from the K^* mass fit. The two-parameter (normalizations for A_0 and $A_\pm$) fit result deviates from 100% longitudinal polarization with a significance of 4.9σ (4.3σ including systematic uncertainties). The significance is defined as $\sqrt{\chi^2_0 - \chi^2_{\rm min}}$, where $\chi^2_{\rm min}$ is the χ^2 value at the best fit and χ^2_0 is the value with the longitudinal polarization fraction set to 100%.

The largest uncertainties in the polarization measurement are due to uncertainties in the nonresonant $\rho K\pi$ PDF, potential scalar-pseudoscalar (S-P) interference, and the nonresonant fraction. We assign a $^{+10.3}_{-0}$% systematic error for the nonresonant PDF. This uncertainty is obtained when we allow up to 1/3 of the ρ helicity PDF to be flat. Interference of the longitudinal amplitude A_0 with

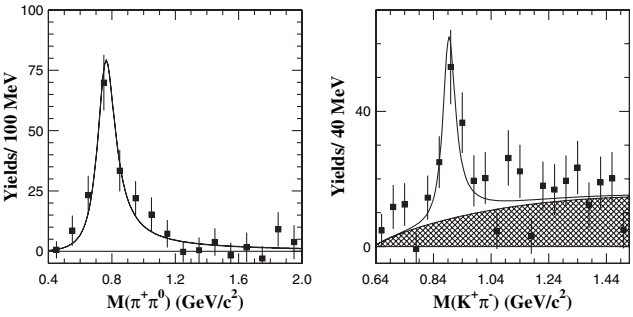

FIG. 2. Signal yields obtained from the $M_{\rm bc}$-ΔE distribution in bins of $M(\pi^+\pi^0)$ (left) for events in the K^{*0} region and in bins of $M(K^+\pi^-)$ (right) for events in the ρ region. Solid curves show the results of the fit. Hatched histograms are for the nonresonant component.

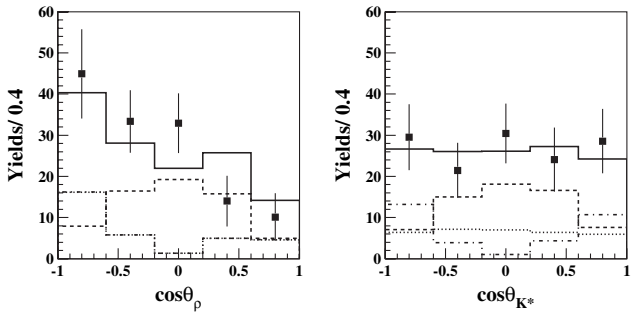

FIG. 3. Fit to background-subtracted helicity distributions. The solid histograms show the results. The dot-dashed (dashed) histograms are the A_0 ($A_\pm$) component of the fit; the dotted histograms are for nonresonant $\rho K\pi$. The low event yield near $\cos\theta_\rho = 1$ is due to the $p_{\pi^0} > 0.4$ GeV/c requirement.

the S-wave $(K\pi)$ system introduces a term with a $2e^{i\Delta\phi}|A_{\rho K\pi}|\cos\theta_{K^*}$ dependence, where $\Delta\phi$ is the phase difference and $|A_{\rho K\pi}|$ is the amplitude of the $B \to \rho K\pi$ decay. The S-P wave interference disappears in the $\cos\theta_\rho$ distribution, which is integrated over $\cos\theta_{K^*}$; however it remains in the $\cos\theta_{K^*}$ distribution. We include an additional linear function for the interference term in the $\cos\theta_{K^*}$ helicity, and redo the χ^2 fit. The resulting small change in f_L, 0.5%, is assigned as the systematic uncertainty for the S-P interference. A $^{+4.0}_{-4.1}$% systematic error is assigned for the uncertainty in the fraction of nonresonant $\rho K\pi$, obtained by varying the nonresonant fraction by $\pm 1\sigma$. Adding the various systematic error contributions in quadrature, we obtain the longitudinal polarization fraction in $B^+ \to \rho^+ K^{*0}$ decays

$$f_L(B^+ \to \rho^+ K^{*0}) = 0.43 \pm 0.11(\text{stat})^{+0.05}_{-0.02}(\text{syst}).$$

To calculate the $B^+ \to \rho^+ K^{*0}$ branching fraction, we use the $M(K\pi)$ invariant mass fit result and MC-determined efficiencies weighted by the measured polarization components. We consider systematic errors in the branching fraction that are caused by uncertainties in the efficiencies of track finding, particle identification, π^0 reconstruction, continuum suppression, fitting, and polarization fraction. We assign an error of 1.1% per track for the uncertainty in the tracking efficiency. This uncertainty is obtained from a study of partially reconstructed D^* decays. We also assign an uncertainty of 0.7% per track on the particle identification efficiency, based on a study of kinematically selected $D^{*+} \to D^0\pi^+$, $D^0 \to K^-\pi^+$ decay. A 4.0% systematic error for the uncertainty in the π^0 detection efficiency is determined from data-MC comparisons of $\eta \to \pi^0\pi^0\pi^0$ with $\eta \to \pi^+\pi^-\pi^0$ and $\eta \to \gamma\gamma$. A 4.5% systematic error for continuum suppression is estimated from studying the process $B^+ \to \bar{D}^0\pi^+$, $\bar{D}^0 \to K^+\pi^-\pi^0$. A $-2.0\%/+1.7\%$ systematic error associated with fits is obtained by shifting each parameter by $\pm 1\sigma$. A 6.7% systematic error for the uncertainty in the $b \to c$ background PDF is obtained by changing the PDF parameterization. A $-4.2\%/+4.4\%$ error due to the uncertainty in the fraction of longitudinal polarization is obtained by varying f_L by its errors. The uncertainty in nonresonant $K^*\pi\pi$ background gives a contribution of $-2.2\%/+0\%$ in addition to $-3.0\%/+2.3\%$ error from uncertainties in the background from other rare B decays. A 7.1% error for possible bias in the χ^2 fit [17] is obtained from a MC study. A 1.1% error for the uncertainty in the number of $B\bar{B}$ events in the data sample is also included. The quadratic sum of all of these errors is taken as the total systematic error. We obtain the branching fraction

$$\mathcal{B}(B^+ \to \rho^+ K^{*0}) = [8.9 \pm 1.7(\text{stat}) \pm 1.2(\text{syst})] \times 10^{-6}.$$

In summary, we have observed the $B^+ \to \rho^+ K^*$ decay with a statistical significance of 5.3σ. We measure the branching fraction to be $[8.9 \pm 1.7(\text{stat}) \pm 1.2(\text{syst})] \times 10^{-6}$. We also perform a helicity analysis and find a substantial transversely polarized fraction $0.43 \pm 0.11(\text{stat})^{+0.05}_{-0.02}(\text{syst})$ with a statistical significance of 4.9σ. The longitudinal polarization fraction f_L measured is similar to the surprisingly low value found in the $b \to s s\bar{s}$ decays $B \to \phi K^*$.

We thank the KEKB group for the excellent operation of the accelerator, the KEK cryogenics group for the efficient operation of the solenoid, and the KEK computer group and the NII for valuable computing and Super-SINET network support. We acknowledge support from MEXT and JSPS (Japan); ARC and DEST (Australia); NSFC (contract No. 10175071, China); DST (India); the BK21 program of MOEHRD and the CHEP SRC program of KOSEF (Korea); KBN (contract No. 2P03B 01324, Poland); MIST (Russia); MHEST (Slovenia); SNSF (Switzerland); NSC and MOE (Taiwan); and DOE (USA).

[1] A. L. Kagan, Phys. Lett. B **601**, 151 (2004).
[2] J. Zhang *et al.* (Belle Collaboration), Phys. Rev. Lett. **91**, 221801 (2003).
[3] B. Aubert *et al.* (*BABAR* Collaboration), Phys. Rev. Lett. **95**, 041805 (2005).
[4] B. Aubert *et al.* (*BABAR* Collaboration), Phys. Rev. Lett. **91**, 171802 (2003); B. Aubert *et al.* (*BABAR* Collaboration), Phys. Rev. Lett. **93**, 231804 (2004).
[5] K. F. Chen *et al.* (Belle Collaboration), Phys. Rev. Lett. **91**, 201801 (2003).
[6] H.-n. Li, Phys. Lett. B **622**, 63 (2005).
[7] Y. Grossman, Int. J. Mod. Phys. A **19**, 907 (2004).
[8] Y. D. Yang, R. M. Wang, and G. R. Lu, Phys. Rev. D **72**, 015009 (2005).
[9] The inclusion of charge conjugate modes is implied unless stated otherwise.
[10] S. Kurokawa and E. Kikutani, Nucl. Instrum. Methods Phys. Res., Sect. A **499**, 1 (2003).
[11] A. Abashian *et al.* (Belle Collaboration), Nucl. Instrum. Methods Phys. Res., Sect. A **479**, 117 (2002).
[12] H. Kakuno *et al.*, Nucl. Instrum. Methods Phys. Res., Sect. A **533**, 516 (2004).
[13] The Fox-Wolfram moments were introduced in G. C. Fox and S. Wolfram, Phys. Rev. Lett. **41**, 1581 (1978). The modified moments used in this Letter are described in S. H. Lee *et al.* (Belle Collaboration), Phys. Rev. Lett. **91**, 261801 (2003).
[14] H. Albrecht *et al.* (ARGUS Collaboration), Phys. Lett. B **241**, 278 (1990).
[15] S. Eidelman *et al.*, Phys. Lett. B **592**, 1 (2004).
[16] K. Abe, M. Satpathy, and H. Yamamoto, hep-ex/0103002.
[17] S. Baker and R. D. Cousins, Nucl. Instrum. Methods Phys. Res., Sect. A **221**, 437 (1984).